Solar Phys (2016) 291:2049–2069
DOI 10.1007/s11207-016-0946-6

Interplanetary Type IV Bursts

A. Hillaris[1] · C. Bouratzis[1] · A. Nindos[2]

Received: 21 December 2015 / Accepted: 21 June 2016 / Published online: 18 July 2016

Abstract We study the characteristics of moving type IV radio bursts that extend to hectometric wavelengths (interplanetary type IV or type IV_{IP} bursts) and their relationship with energetic phenomena on the Sun. Our dataset comprises 48 interplanetary type IV bursts observed with the *Radio and Plasma Wave Investigation* (WAVES) instrument onboard *Wind* in the 13.825 MHz – 20 kHz frequency range. The dynamic spectra of the *Radio Solar Telescope Network* (RSTN), the *Nançay Decametric Array* (DAM), the *Appareil de Routine pour le Traitement et l' Enregistrement Magnetique de l' Information Spectral* (ARTEMIS-IV), the *Culgoora*, *Hiraso*, and the *Institute of Terrestrial Magnetism, Ionosphere and Radio Wave Propagation* (IZMIRAN) *Radio Spectrographs* were used to track the evolution of the events in the low corona. These were supplemented with soft X-ray (SXR) flux-measurements from the *Geostationary Operational Environmental Satellite* (GOES) and coronal mass ejections (CME) data from the *Large Angle and Spectroscopic Coronagraph* (LASCO) onboard the *Solar and Heliospheric Observatory* (SOHO). Positional information of the coronal bursts was obtained by the *Nançay Radioheliograph* (NRH). We examined the relationship of the type IV events with coronal radio bursts, CMEs, and SXR flares. The majority of the events (45) were characterized as compact, their duration was on average 106 minutes. This type of events was, mostly, associated with M- and X-class flares (40 out of 45) and fast CMEs, 32 of these events had CMEs faster than

Electronic supplementary material The online version of this article (doi:10.1007/s11207-016-0946-6) contains supplementary material, which is available to authorized users.

✉ A. Hillaris
ahilaris@phys.uoa.gr

C. Bouratzis
kbouratz@phys.uoa.gr

A. Nindos
anindos@cc.uoi.gr

1 Section of Astronomy, Astrophysics and Mechanics, Department of Physics, University of Athens, 15783 Athens, Greece

2 Section of Astro-geophysics, Department of Physics, University of Ioannina, 45110 Ioannina, Greece

1000 km s^{-1}. Furthermore, in 43 compact events the CME was possibly subjected to reduced aerodynamic drag as it was propagating in the wake of a previous CME. A minority (three) of long-lived type IV_{IP} bursts was detected, with durations from 960 minutes to 115 hours. These events are referred to as extended or long duration and appear to replenish their energetic electron content, possibly from electrons escaping from the corresponding coronal type IV bursts. The latter were found to persist on the disk, for tens of hours to days. Prominent among them was the unusual interplanetary type IV burst of 18 – 23 May 2002, which is the longest event in the *Wind*/WAVES catalog. The three extended events were typically accompanied by a number of flares, of GOES class C in their majority, and of CMEs, many of which were slow and narrow.

Keywords Radio bursts · Dynamic spectrum · Meter and longer wavelengths · Coronal mass ejections

1. Introduction

Solar metric radio bursts provide a unique diagnostic of the development of flare events accompanied by coronal mass ejections (CME) in the low corona, flare-CME events from now on. Their onset and evolution is accompanied by energetic-particle acceleration and injection into interplanetary (IP) space as well as shocks (see *e.g.* the review by Pick and Vilmer, 2008; Nindos *et al.*, 2008). Their signatures at metric to kilometric wavelengths trace disturbances propagating from the low corona to the interplanetary space.

Three types of nonthermal radio bursts are associated with the flare-CME events (Sakurai, 1974; White, 2007; Gopalswamy, 2011):

- Bursts of the type III family. They are produced by energetic electrons accelerated in the Sun and traversing the solar atmosphere, along coronal magnetic lines rooted in its surface. In open field lines, they may escape into the interplanetary space (see, for example, Figure 1 of Klein *et al.*, 2008, also Alissandrakis *et al.*, 2015). In the dynamic spectra, these standard type III bursts appear as fast-drifting bands ($\mathrm{d}f/f\,\mathrm{d}t \approx 1.0$ s^{-1}). When trapped in closed magnetic structures, they eventually turn toward the Sun, resulting in inverted U- or J-shaped bursts in the dynamic spectra (hence U- or J-type bursts of the type III family). In flare-CME events, the transition from the type U and J bursts to the typical type III often marks the restructuring, or opening, of the magnetic field lines as originally confined, energetic electrons gain access to open magnetic lines. An example of dynamic radio spectra showing this transition from U- and J-type bursts to a standard type III burst at the beginning of the 17 January 2005 event can be found in Hillaris *et al.* (2011). In the hectometric and kilometric regime, long-duration storms of individual type III bursts (Fainberg and Stone, 1970a,b, 1971; Bougeret, Fainberg, and Stone, 1983) covering several days (5.4 on average according to Kayser *et al.*, 1987) were recorded. These are different from the hectometric–kilometric extensions of type III bursts and are known as IP storms and, more often than not, may appear as storm continua on the dynamic spectra. The individual type III components of the IP storms (micro-type III bursts, according to Morioka *et al.*, 2007) are significantly weaker than the typical type III bursts in the same frequency range. The IP storms are well associated with active regions (Kayser *et al.*, 1987), but the micro-type III bursts are not accompanied by significant

soft X-ray (SXR) flare activity. This implies the need of a persistent coronal store of suprathermal electrons (Bougeret, Fainberg, and Stone, 1984a,b) supplying this type of activity.

- Type II bursts. They are the radio signatures of the passage of a magneto-hydrodynamic (MHD) shock wave through the tenuous plasma of the solar corona; their radio emission is due to energetic electrons accelerated at the shock front. It is in general accepted that type II bursts at decametric and longer wavelengths are driven by CME bows or flanks (Vršnak and Cliver, 2008). At the metric range, on the other hand, they might be also due to flare blasts, in addition to CMEs (Cane and Reames, 1988; Nindos *et al.*, 2011; Magdalenić *et al.*, 2010, 2012), or to reconnection outflow termination-shocks (Aurass, Vršnak, and Mann, 2002).
- Type IV bursts. They are radio continua caused by the radiation of energetic electrons trapped within magnetic structures and plasmoids. They have been recorded in almost all frequency ranges starting from the microwaves as type IVμ bursts and the decimetric range as type IVdm bursts (Benz, 1980). In the metric wavelengths the type IVm bursts are divided into moving (IVmA or IVM) and stationary (IVmB). The type IVmB bursts emanate from stationary magnetic structures that are typically located above active regions or post-eruption arcades behind CMEs (Robinson, 1985; Gopalswamy, 2011). The type IVm burst are sometimes referenced as flare continua (FCM when preceding a type IVmA or FCII when following a type II burst, see Robinson, 1978). They are also identified as continuum noise storms (type IVsA and IVsB, corresponding to type IVmA and IVmB, see discussion in Sakurai, 1974, and their Figure 14). The type IVmA bursts (Boischot, 1957) appear to be moving outward at velocities of about $100-1000\ \mathrm{km\,s^{-1}}$, which are comparable to CME speeds (White, 2007); they sometimes last more than ten minutes. A number of these are believed to originate within the densest substructures of CMEs (Klein and Mouradian, 2002; Bastian *et al.*, 2001; Aurass *et al.*, 1999; Bain *et al.*, 2014). These substructures might be erupting prominences within the CMEs. The type IVmA burst – CME association was found to increase with the speed of the CME (Gergely, 1986, and references therein). A subset of the moving type IV radio bursts extend in dynamic spectra to the hectometric wavelengths (frequencies lower than $\approx$20 MHz) and are recorded with the *Radio and Plasma Wave Investigation* (WAVES) instrument onboard *Wind*; these are interplanetary type IV or $\mathrm{IV_{IP}}$ radio bursts.

In this article we examine the characteristics and the evolution of interplanetary type IV bursts and their relationship with energetic phenomena on the Sun such as flares and CMEs. The data used are from the *Wind*/WAVES receivers and a number of ground-based instruments. From the combined datasets an extensive table of type $\mathrm{IV_{IP}}$ and associated activity was compiled and is presented as supplementary online material (file IPtypeIV.pdf). A detailed description of the table is included in the Appendix. The question addressed in our study is twofold. First, we examine the association of these bursts with intense flares and fast CMEs, examining whether they may be considered as another aspect of the big flare syndrome first introduced by Kahler (1982). Second, we search for other processes affecting, totally or partially, the appearance of this type of radio bursts.

This report on interplanetary type IV (or type $\mathrm{IV_{IP}}$) bursts is structured as follows. In Section 2 we describe the instrumentation and datasets used in our study. The data analysis is presented in Section 3, including an overview of selected events in Sections 3.3, 3.4, and 3.5. In Section 4 we present the characteristics and the evolution of different types of type $\mathrm{IV_{IP}}$ events, which are then discussed in Section 5. The conclusions are presented in the same section.

2. Observations and Data Selection

The basic data used in this study are dynamic spectra recorded by the R1 and R2 receivers of the *Wind*/WAVES (Bougeret *et al.*, 1995) in the 20 kHz – 13.825 MHz frequency range from 1998 to 2012. The interplanetary type IV bursts selected were previously identified in the *Wind*/WAVES online catalog.[1] The observations were complemented by data in the metric and decametric wavelengths from the following ground-based radio observatories:

- The ARTEMIS-IV[2] radio spectrograph (Caroubalos *et al.*, 2001; Kontogeorgos *et al.*, 2006a,b, 2008) observes in the frequency range 20 – 650 MHz.
- The *Culgoora Radio Spectrograph* (Prestage *et al.*, 1994) observes in the frequency range 18 – 1800 MHz.
- The *Nançay Decametric Array*[3] (DAM: Boischot *et al.*, 1980; Lecacheux, 2000) observes in the range 20 – 75 MHz.
- *The Nançay Radioheliograph* (NRH: Kerdraon and Delouis, 1997) provides daily, 09:00 – 15:30 UT, two-dimensional images of the Sun at ten frequencies from 450 to 150 MHz with sub-second time resolution. It was used for positional information of the metric–decametric radio emission. In this article the quick-look-style NRH data from the radio-monitoring site[4] were used.
- The *Hiraiso Radio Spectrograph*[5] (HiRAS: Kondo *et al.*, 1995) observes in the frequency range 25 – 2500 MHz.
- *The Institute of Terrestrial Magnetism, Ionosphere and Radio Wave Propagation* (IZMIRAN) *Radio Spectrograph*[6] (Gorgutsa *et al.*, 2001) observes in the range 25 – 270 MHz.
- *The Radio Solar Telescope Network*[7] (RSTN: Guidice *et al.*, 1981) with a number of solar radio observatories at various locations around the world guarantees full 24-hour coverage:
  - Sagamore Hill at Hamilton, Massachusetts, USA (42°33′N 70°49′W);
  - Palehua at Kaena Point, Hawaii (21°24′N 158°06′W);
  - Holloman at New Mexico, USA (32°51′N 106°06′W);
  - Learmonth at Western Australia, Australia (22°13′S – 114°06′E);
  - San Vito dei Normanni, Italy (40°39′N 17°42′E).

  These observatories provide dynamic spectra in the 25 – 180 MHz range.

Additional datasets were used to examine the association of the type IV_{IP} bursts with the evolution of flares and CMEs:

- CME data from the *Large Angle and Spectroscopic Coronagraph* (LASCO) Catalog online[8] (Yashiro *et al.*, 2004; Gopalswamy *et al.*, 2009).

[1] www.lep.gsfc.nasa.gov/waves/data_products.html.

[2] *Appareil de Routine pour le Traitement et l' Enregistrement Magnetique de l' Information Spectral*, http://artemis-iv.phys.uoa.gr/.

[3] bass2000.obspm.fr/home.php.

[4] http://radio-monitoring.obspm.fr/nrh_data.php.

[5] sunbase.nict.go.jp/solar/denpa/index.html.

[6] www.izmiran.ru/stp/lars/.

[7] ftp://ftp.ngdc.noaa.gov/STP/space-weather/solar-data/solar-features/solar-radio/rstn-spectral.

[8] http://cdaw.gsfc.nasa.gov/CME_list.

- SXR characteristics such as online reports[9] and light curves[10] from the *Geostationary Operational Environmental Satellite* (GOES).
- Images from the *Extreme Ultraviolet Imaging Telescope* (EIT: Delaboudinière *et al.*, 1995) onboard the *Solar and Heliospheric Observatory* SOHO. They were used to provide information on flare positions.

From the *Wind*/WAVES catalog all events indicated as bursts of type IV_{IP} (48 in total) were selected. Many (36) were accompanied by interplanetary type II shocks.

A comprehensive list of the interplanetary type IV bursts and the associated activity including, but not restricted to, coronal burst, flare, and CME characteristics is attached as supplementary online material (file IPtypeIV.pdf). A detailed description of the table is included in the Appendix. In compiling this catalog, we included information of all the *Wind*/WAVES type IV_{IP} bursts, their associated CMEs and SXR flares in the 1998 – 2012 period, and the accompanying interplanetary type II and coronal type II, IV, and III bursts. The above-mentioned CMEs that are thought to drive the type IV_{IP} bursts are referred to as main CMEs to distinguish them from preceding CMEs along the same path; the latter were included in the table as they may affect the appearance of type IV_{IP} bursts, as discussed in Sections 4.1 and 5. The selection of the CMEs preceding the main ejection along the same path is based on a time interval of about 48 hours before the main CME and whether the sectors (or cones in 3D) defined by position angle and width for the main and the preceding CME overlap. Occasionally, more than one preceding CME is included in the catalog because they are all within the 48 hours window and appear to overlap in part with the main CME. The overlap criterion is relaxed when one or both the main and the preceding CMEs are halo CMEs; in this case we assume that an overlap is always possible, at least in part.

3. Data Analysis

3.1. Data Processing

The combination of hectometric dynamic spectra by *Wind*/WAVES with metric and decametric spectra from the ground-based radio spectrographs (see Section 2) was first plotted as a composite dynamic spectrum. These were found to include an amount of features, mostly groups of type III and II bursts, embedded in a slowly varying background. Often the continuum background was removed by the use of differentiation of the dynamic spectra in time domain. This filtering, however, amplifies the high-frequency noises, therefore the smoothed differentiation filter of Usui and Amidror (1982) was used. This simultaneously performs a smoothing and differentiation, so that it can be regarded as a low-pass differentiation filter (digital differentiator) appropriate for experimental (noisy) data processing.

The composite dynamic spectra provide an overview of the evolution of the type IV_{IP} bursts under study and of the accompanying radio activity, from the corona to the interplanetary space. On each dynamic spectrum several time-histories were superposed:

- The approximate frequency–time trajectories of the CME fronts. These were plotted on the dynamic spectra, using the coronal density model of Vršnak, Magdalenić, and Zlobec (2004), as thick-dotted lines. The details of the model are presented in Section 3.2. The linear fits to the height–time trajectories of the CME fronts, from the LASCO images,

[9] ftp://ftp.ngdc.noaa.gov/STP/space-weather/solar-data/solar-features/solar-flares/x-rays/ and https://solarmonitor.org/data.

[10] http://satdat.ngdc.noaa.gov/sem/goes/data/.

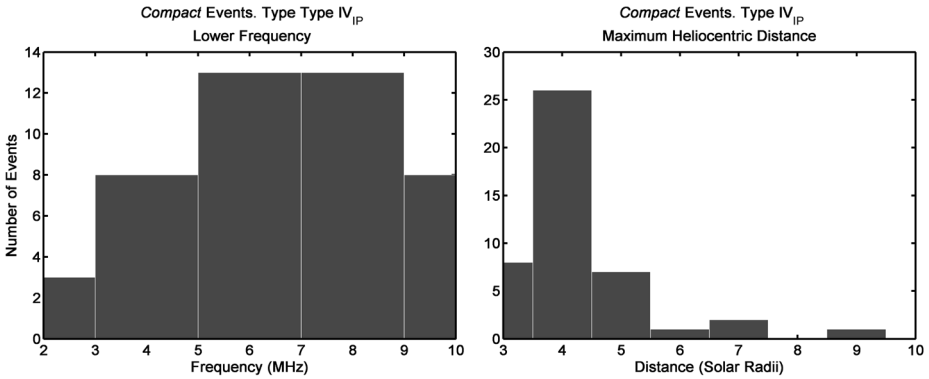

Figure 1 Left panel: distribution of the low-frequency limit of the compact interplanetary type IV bursts. Right panel: the corresponding heliocentric distance of these type IV bursts based on the low-frequency limit and the model dependent calculations described in Section 3.2.

were converted into the frequency–time traces of the fundamental and harmonic plasma emission; the squares mark the measured positions of the CME front.

- The GOES SXR time-profiles. The solid black (1.0 – 8.0 Å) and the thick-dotted magenta (0.5 – 4.0 Å) curves display the SXR time history describing thermal emission from the hot flare plasma.

Of the 48 type IV$_{IP}$ bursts in this article, 17 overlapped at least partly with the NRH window of observation. For these, the position of the coronal extension (metric type IV burst) of the interplanetary burst was compared to the SXR flare position and the solar sources of the CME in the EIT images. Their spatial relationship was established combining NRH radio contours overlayed on the EIT 195 Å difference image and LASCO difference image. Two categories of type IV$_{IP}$ bursts were found:

Compact type IV$_{IP}$ bursts. These were mostly associated with M- and X-class flares and fast CMEs; their duration was on average 100 ($\pm$11) minutes. Their minimum frequency was in the 10 – 2 MHz range, which corresponds to 3 – 10 $R_{\odot}$ heliocentric distances. The distribution of the low-frequency limits and the corresponding distances, derived from the calculations in Section 3.2, are exhibited in Figure 1. In total, 45 of these events were found in the *Wind*/WAVES lists. An example is presented in Section 3.3.

Long-duration or extended type IV$_{IP}$ bursts. They represent a small minority of three events with durations from 960 minutes to 115 hours. Their morphology was found to be less uniform than that of their counterparts. Two of them (catalog numbers 34, 18 – 23 May 2002, and 45, 27 May 1999, described in Sections 3.4 and 3.5) were accompanied by a sequence of small flares and slow and narrow CMEs with an occasional medium or large flare within the sequence. Another event (number 14, 17 January 2005, presented in Section 3.6) originated from a fast CME and large flare, but extended far beyond the duration of a compact event.

The distribution of the interplanetary type IV bursts duration is presented in Figure 2 for all the events of the study. The three extended events are the outliers of the histogram in the left panel. The distribution of the duration of the compact events is also presented separately in the right panel of Figure 2. In Section 4 the differences between the characteristics of the extended and the compact events are examined and discussed, except for their duration.

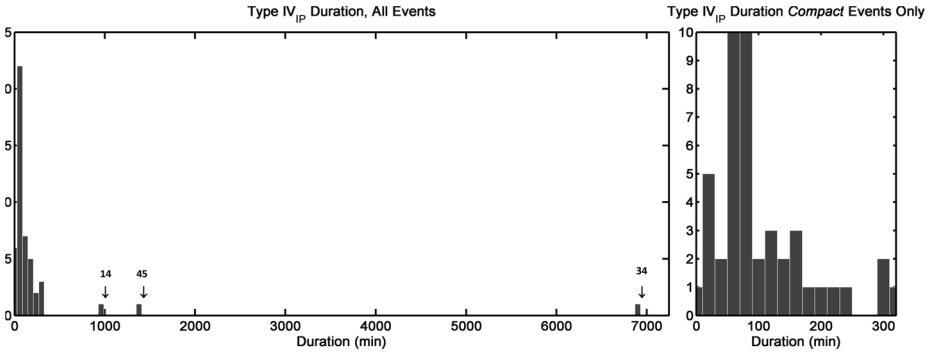

Figure 2 Distribution of the duration of the interplanetary type IV bursts. Left panel: all (48) events; the three extended events are pointed with arrows. Their catalog numbers are shown above them. Right panel: histogram including only the 45 compact events.

3.2. Coronal Density-Height Model Selection

As plasma emission depends on the electron density, which in turn may be converted into a coronal height using density models, we may calculate the radio source heights and speeds from the dynamic spectra. The establishment of a correspondence between frequency of observation-coronal height and frequency drift rate-radial speed is affected by ambiguities introduced by the variation of the ambient medium properties. These may be the result of the burst exciter propagation in the undisturbed plasma, overdense or underdense structure or CME afterflows (see Pohjolainen *et al.*, 2007; Pohjolainen, Hori, and Sakurai, 2008, for a detailed discussion on model selection).

The density model of Vršnak, Magdalenić, and Zlobec (2004),

$$\frac{n}{10^8\ \mathrm{cm}^{-3}} = 15.45\left(\frac{R_\odot}{R}\right)^{16} + 3.165\left(\frac{R_\odot}{R}\right)^{6} + 1.0\left(\frac{R_\odot}{R}\right)^{4} + 0.0033\left(\frac{R_\odot}{R}\right)^{2},$$

which describes the coronal density behavior well in the wide range of distances from the low corona to interplanetary space was used to convert the linear fits to the height–time trajectories of the LASCO CME fronts to frequency–time tracks on the composite dynamic spectra.

3.3. Overview of the 2 May 1998 Compact Event Evolution

The 2 May 1998 compact event (catalog number 47) is typical of its class. It has drawn considerable attention due to the large number of instruments that have observed it, including *Wind*/WAVES, LASCO, EIT, NRH, and several radio spectrographs. It is reported in a number of articles that mainly focused on the solar surface magnetic waves (Zharkova and Kosovichev, 1999), the pre-CME launch activity (Pohjolainen, Khan, and Vilmer, 1999), and the on-disk development of the CME (Pohjolainen *et al.*, 2001).

The interplanetary type IV event (see composite spectrum in Figure 3) starts at 14:10 UT on 02 May and lasts until 15:40 UT of the same day in the frequency range 8 – 14 MHz. An interplanetary type II burst was recorded from 14:25 – 14:50 UT in the 3 – 5 MHz range of *Wind*/WAVES. In the catalog it is described as a narrowband wisp, but it is well associated

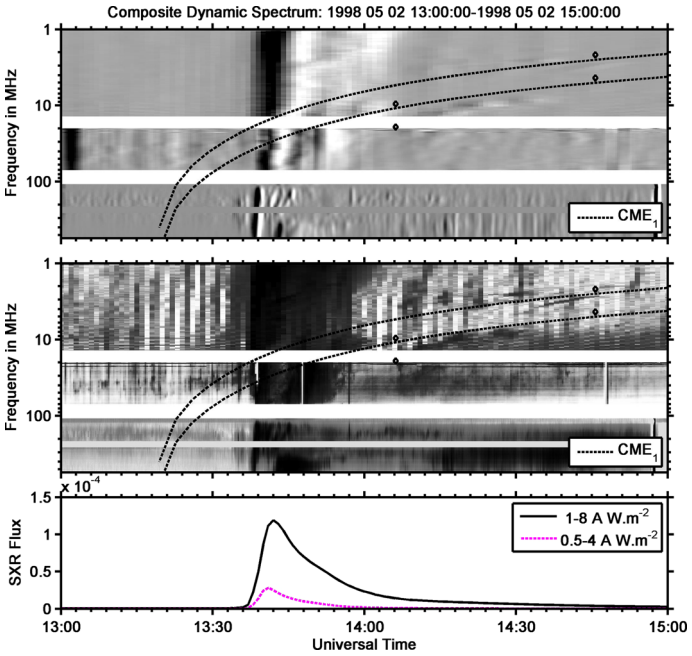

Figure 3 02 May 1998 event. Top panel: *Wind*/WAVES and ARTEMIS-IV differential spectrum (inverse grayscale). Middle panel: dynamic (intensity, inverse grayscale) spectrum. The frequency–time plots derived from the linear fit to the front trajectory of the associated CME and an empirical density model (see Section 3.2) for the fundamental and harmonic (thick-dotted curves) plasma emission are overlaid on the spectra. Bottom panel: the profiles of GOES SXR 1 – 8 Å (solid black line) and 0.5 – 4 Å (thick-dotted magenta line) flux.

with the front of the CME. Another type II, without apparent association with the CME front, appears in the 6 – 400 MHz range, recorded by the ARTEMIS-IV, the *Nançay Decametric Array* (DAM), and the *Wind*/WAVES from 13:30 – 13:46 UT. The event exhibits a multiple band structure and was first reported by Pohjolainen *et al.* (2001). The high-frequency extension of the type IV_{IP} was recorded by the DAM and the ARTEMIS-IV radio spectrographs and extended above the 500 MHz (see also Pohjolainen *et al.*, 2001, their Figure 8). This activity is accompanied by an X1.1/3B-class flare from active region (AR) 8210 at heliographic coordinates S15W15; the flare started at 13:31 and ended at 13:51 UT, peaking at 13:42 UT.

The NRH records at 432 and 164 MHz indicate that the type IV continuum appeared over AR 8210 and, in the 164 MHz images, started moving northward at 13:34 UT. This is consistent with the motion of a rather fast, 938 km s^{-1}, halo CME (first viewed at 14:06 UT, back-extrapolated lift-off at 13:07 UT) with measured position angle 331° (see Figure 4). This CME appears to drive the fundamental and harmonic pair mentioned in the previous paragraph. As regards the CME path, there were two preceding halo CMEs on 02 May 1998 at 05:32 UT and on 01 May 1998 at 23:40 UT.

The broadband dynamic spectra and the NRH images indicate that the compact interplanetary type IV burst is associated with an X-class flare and the fast halo-CME. The latter propagates in the wake of a previous halo-CME that was launched approximately 8.5 hours before. This example represents the combined effects of an intense flare and a fast CME with the CME propagating within a low-drag region due to the passage of a previous CME.

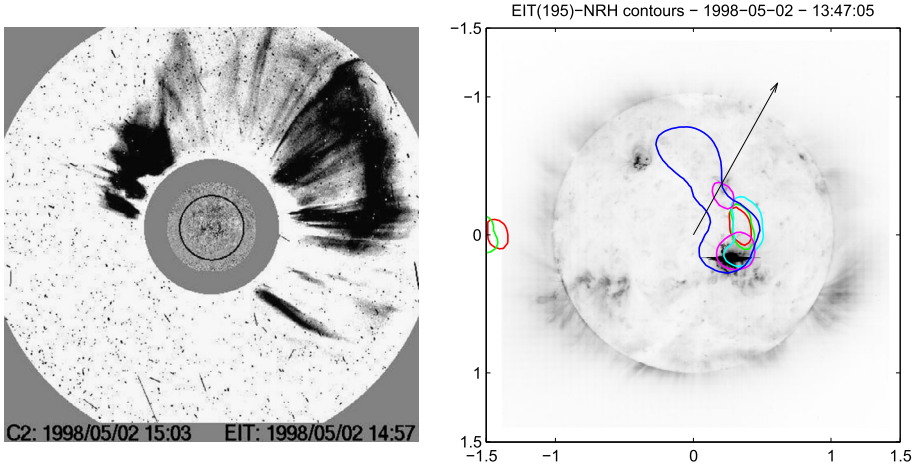

Figure 4 Left: LASCO and EIT 195 Å running-difference frames of the 02 May 1998 14:06 UT CME (inverse grayscale). Right: NRH half-power contours (at 432 (red), 410 (green), 327 (cyan), 236 (magenta), and 164 (blue) MHz). The contours were recorded at successive times starting with 432 MHz at 13:47:05 UT to 164 MHz at 13:51:53 UT, thus tracing the outward motion of the type IV burst. The arrow indicates the halo-CME measured position angle from the LASCO catalog.

3.4. Overview of the 18 – 22 May 2002 Extended Event Evolution

The type IV_{IP} event started at 09:00 UT on 18 May and lasted until 04:00 UT on 23 May in the frequency range 0.3 – 9 MHz (catalog number 34). It was the only such event observed by *Wind*/WAVES in its years of operation (Reiner *et al.*, 2006). An interplanetary type II burst was recorded from 22 May at 04:10 UT until 23 May 10:10 UT in the 0.03 – 0.5 MHz range. The *Wind*/WAVES dynamic and differential spectra, with the CME front trajectories overlaid, and the SXR flux are exhibited in Figure 5; details in the period 07:45 – 12:45 UT on 19 May are presented in Figure 6. This event was briefly reported by Gopalswamy (2004), who, based on polarization measurements, considered it as a hectometric storm continuum and not a type IV_{IP} burst, as reported in the *Wind*/WAVES catalog.

On the solar disk, we see a number of active-region complexes in the 18 – 23 May period. When the continuum emission started, on 18 May AR 9957 (N08E47) was the largest and most complex region on the disk. This region was accompanied by AR 9958 (N04E45) and followed by AR 9960 at N05E74 and AR 9962 and AR 9963, which appeared on 21 May at N15E47 and N17E63, respectively. South of this group were AR 9954 (S22E35), AR 9955 (S14E37), and in the western hemisphere AR 9945 (S02W73), AR 9948 (S21W20), and AR 9950 (S05W42). In the left panel of Figure 7 we present the positions of all SXR flares within the 18 – 23 period and of the corresponding active regions.

Throughout the period of interest from 18 May 2002 at 02:44 UT to 23 May 2002 at 04:00 UT, 38 SXR flares were recorded by GOES; positional data were obtained for 33 of them. The AR 9957, AR 9958, AR 9960, AR 9962, and AR 9963 complex, located in the NE quadrant of the disk, produced 10 C-class and one M1.5 SXR flares. The single AR 9961 in the SE quadrant produced 16 flares (including an X2.1 and an M5.0) on 19 May 2002 at 15:54 UT. Within the same period, 24 CMEs were recorded in the LASCO catalog. The position angles, shown in the right panel of Figure 7, indicate that they emerged from all quadrants of the solar disk. This activity was associated with many type III burst-groups,

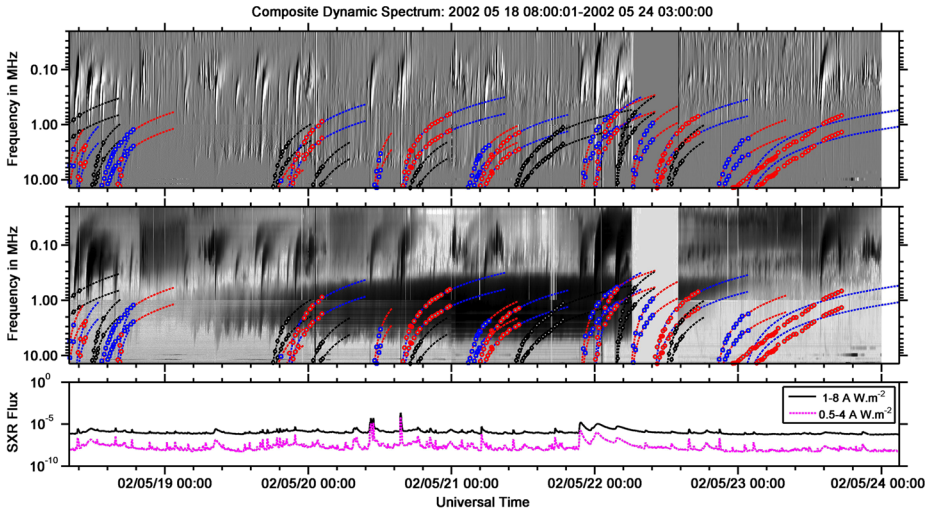

Figure 5 18 – 22 May 2002 event (18:08:00 UT on 18 May to 00:03:00 UT on 23 May). Top panel: *Wind*/WAVES differential spectrum (inverse grayscale). Middle panel: dynamic (intensity, inverse grayscale) spectrum. The frequency–time plots derived from the linear fits to the front trajectory of the associated CMEs and the density model presented in Section 3.2 for the fundamental and harmonic (thick-dotted curves) plasma emission are overlaid on the spectra. In this example, the CME trajectories are shown with different colors. The squares that mark the positions of the CME fronts are drawn in black on the black trajectories, in red on the blue trajectories, and in blue on the red trajectories (see Section 3.1). Bottom panel: the profiles of GOES SXR 1 – 8 Å (solid black line) and 0.5 – 4 Å (thick-dotted magenta line) flux. The time is written in the format date, hours, and minutes.

2 – 3 type II shocks in the metric range (see the table included as supplementary online material), and a persistent continuum appearing in the NE quadrant over the AR 9957, AR 9958, AR 9960, AR 9962, and AR 9963 group during the 19 – 23 May period. The metric and decametric continuum appears in the SW quadrant, over AR 9948, only on 18 May (see Figure 8); on this day, it coexisted with the persistent continuum (over the AR 9957) mentioned above.

The SXR activity originates mostly in the NE (AR 9957, AR 9958, AR 9960, AR 9962, and AR 9963) and the SE (AR 9961) quadrants; most of the CME position angles indicate ejections from the same two quadrants (see Figure 7, right panel). The position of the type III bursts that could be localized were almost equally divided between the SE and NE quadrants, but the vast majority clearly appears to continue into the *Wind*/WAVES hectometric range in the differential spectra at frequencies lower than those of the type IV_{IP}. Furthermore, the type III and CME activity continues past the end of the interplanetary type IV burst. The metric continuum, on the other hand, appears persistently in the NRH images on top of the group formed by AR 9957, AR 9958, AR9960, AR 9962, and AR 9963 from 19 to 23 May. This implies a steady coronal reservoir of energetic electrons, which may follow the magnetic lines trailing CMEs originating at the NE quadrant and replenish the electrons of the interplanetary type IV_{IP} burst.

3.5. Overview of the 27 – 28 May 1999 Extended Event Evolution

The event started on 27 May 1999 at 10:55 UT and ended on 28 May at 15:00 UT (catalog number 45). The event was composed of interplanetary type II/IV bursts having both coro-

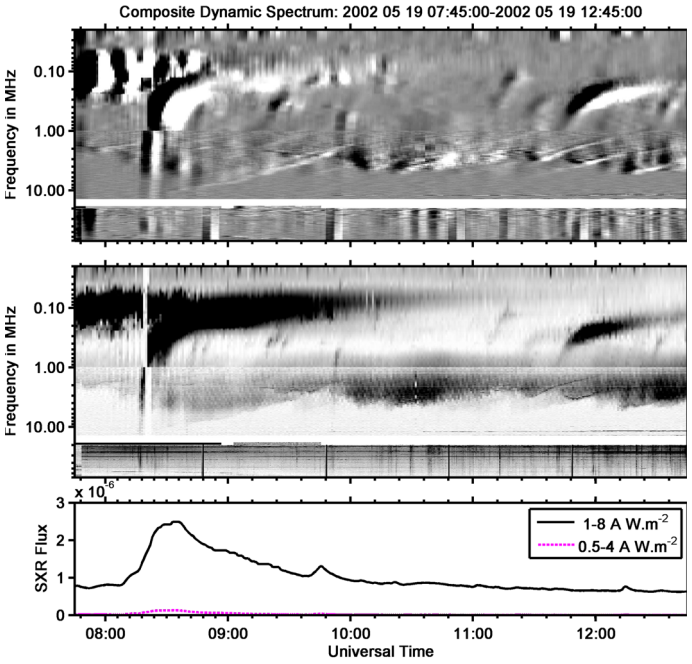

Figure 6 18 – 22 May 2002 event showing details on 19 May from 07:45 UT to 12:45 UT. The dynamic spectra are combined records from *Wind*/WAVES and DAM, extended in the 0.02 – 70 MHz range. Top panel: differential spectrum (inverse grayscale). Middle panel: dynamic (intensity, inverse grayscale) spectrum. Bottom panel: the profiles of GOES SXR 1 – 8 Å (solid black line) and 0.5 – 4 Å (thick-dotted magenta line) flux.

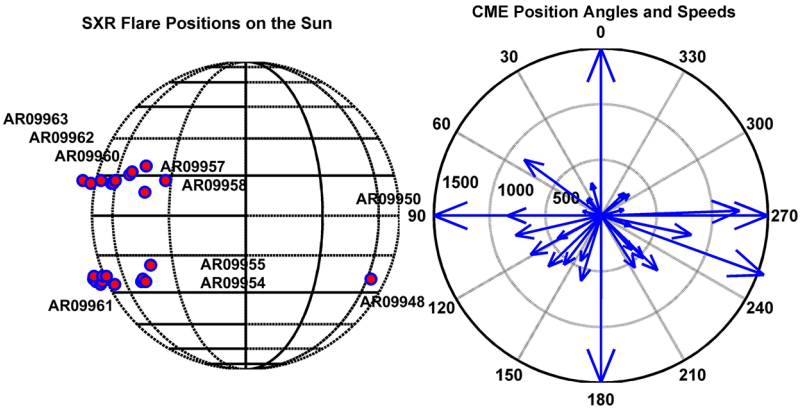

Figure 7 Left: Positions of the SXR flares (purple dots with blue border) and active regions. The AR positions, indicated approximately by their names, are taken from the SolarMonitor (http://www.solarmonitor.org) on 20 May 2002. Right: CME position angles and speeds indicated with segments ending in an arrowhead. The segment length is proportional to the CME speed. The flare and CME positions extend throughout the whole 18 – 23 May 2002 period.

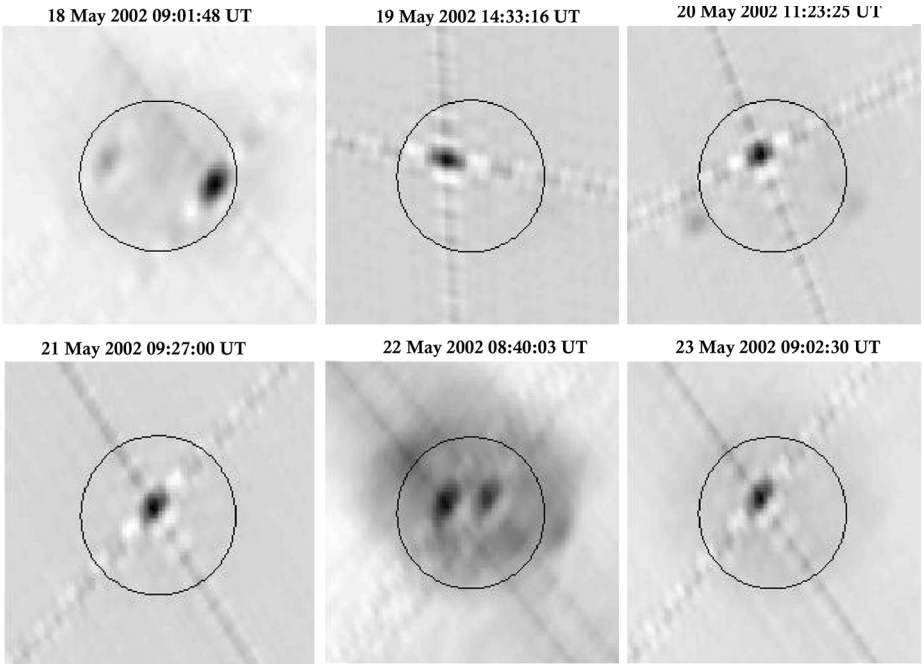

Figure 8 Positions of the coronal type IV bursts in the 18 – 23 May 2002 period, obtained with the *Nançay Radioheliograph* at 164 MHz.

nal extensions. This event was accompanied by a number of C-class SXR flares and narrow CMEs. An overview including the *Wind*/WAVES dynamic spectrum, the CME front trajectories, and the SXR flux profiles is presented in Figure 9. There are only two wide CMEs, a halo CME on 27 May at 11:06 UT and a rather wide CME on 28 May at 10:26 UT, which almost mark the start and the end of the event. Figures 10 and 11 show details of this event in different time periods on 27 and 28 May.

Similar to the 18 – 22 May 2002 event, in Section 3.4, there was also a persistent coronal type IV burst, which appeared over AR 8552 (N18E31) in the NRH records. This region remained active throughout the duration of the interplanetary type IV burst, and most of the small SXR flares and a number of type III bursts originated from it as well. In Figure 12 we present the position of the coronal type IV burst on 27 and 28 May in NRH images. There is also a long series of type III bursts and groups that covers the type IV_{IP} interval. Most of these type III bursts, however, overshoot the type IV_{IP} continuum, so that we expect that the main source of energetic electrons is its coronal counterpart persisting over AR8552.

3.6. Overview of the 17 January 2005 Extended Event Evolution

On 17 January 2005, two fast CMEs were recorded in close succession during two distinct episodes of a 3B/X3.8 flare in AR 10720. The type IV_{IP} burst started at 10:55 UT on 17 January and ended on 18 January at 02:00 UT (event catalog number 14); for an overview of the dynamic spectrum see Figure 3 of Hillaris *et al.* (2011). The coronal extension of the type IV_{IP} burst was found to originate from AR10720 and persisted throughout the duration of its interplanetary counterpart. The type II activity, on the other hand, was restricted to the frequency range below 14 MHz. The type III groups accompanying the event were found

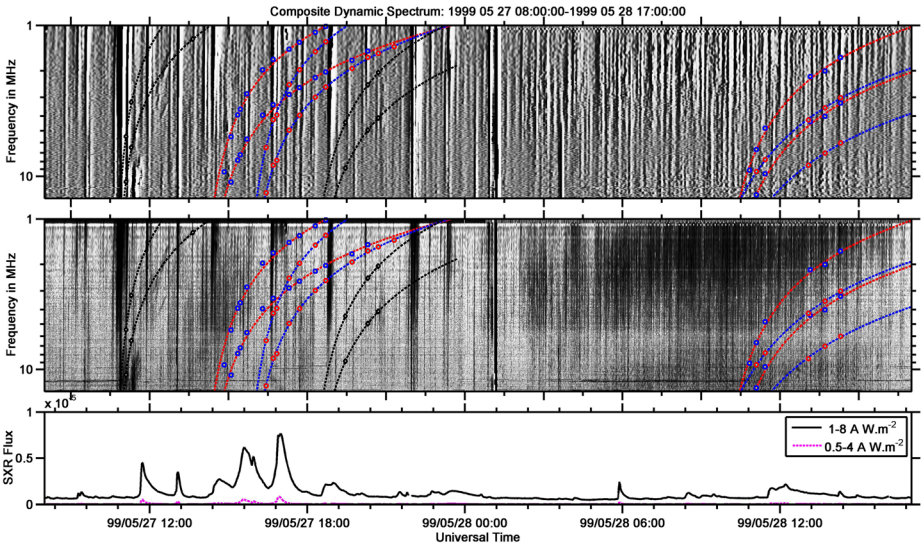

Figure 9 27 – 28 May 1999 event in the period from 27 May 08:00 UT to 28 May 17:00 UT. Top panel: *Wind*/WAVES differential spectrum (inverse grayscale). Middle panel: dynamic (intensity) spectrum. The frequency–time plots derived from the linear fits to the front trajectories of the associated CMEs and an empirical density model (see Section 3.2) for the fundamental and harmonic (thick-dotted curves) plasma emission are overlaid on the spectra. In this example, the CME trajectories are shown with different colors. The squares that mark the positions of the CME fronts are drawn in black on the black trajectories, in red on the blue trajectories, and in blue on the red trajectories (see Section 3.1). Bottom panel: the profiles of GOES SXR 1 – 8 Å (solid black line) and 0.5 – 4 Å (thick-dotted magenta line) flux. The time is in the format date, hours, and minutes.

to overshoot the low-frequency limit of the type IV_{IP} burst at least after 08:18 UT. Earlier, groups of U-type bursts and type IV fine structures indicated acceleration and partial trapping of electrons behind the CME front.

A detailed study of the radio signatures of this event (Table 1 in Hillaris *et al.*, 2011, which presents a comprehensive outline of its time evolution) points toward possible multiple acceleration mechanisms. These include CME associated shocks in the high corona and the interplanetary space and also shock-independent accelerators at low altitudes associated with the type IV continuum behind the CME.

This event had distinct features of the compact class, *i.e.* it was associated with an intense flare and two fast CMEs, but its long duration characterizes it as extended. Similar to the previous two long-duration events, energetic electrons provided by low corona sources could be associated with the coronal type IV burst.

4. Characteristics of All the Events

4.1. Characteristics of the 45 Compact Events

Of the 48 type IV_{IP} bursts of our sample 45, classified as compact, were found to conform to the big flare syndrome, which suggests that, statistically, energetic phenomena are more intense in larger flares, regardless of the detailed physics. Nineteen were associated with

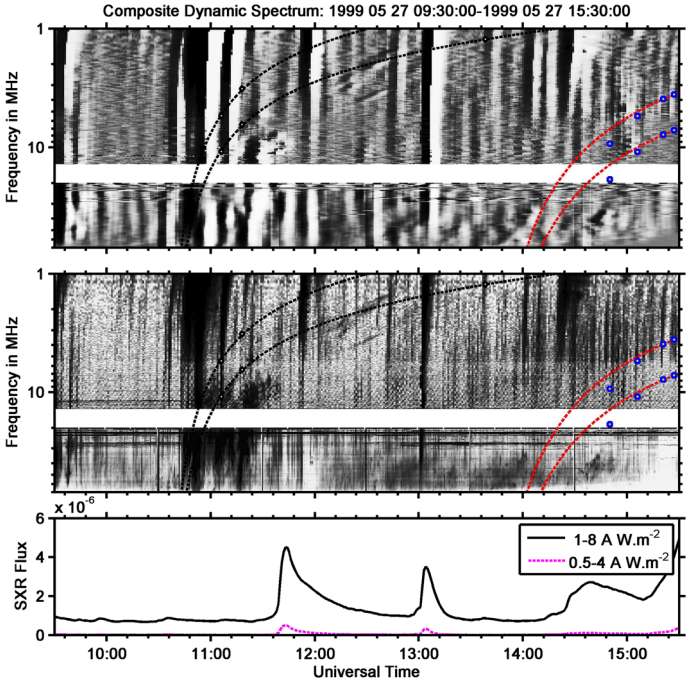

Figure 10 27 – 28 May 1999 event. The panels show the event in the 27 May 09:30 – 15:30 UT period. The dynamic spectra are combined records from the *Wind*/WAVES and the DAM in the 1 – 70 MHz range. This section of the type IV_{IP} starts above 70 MHz and extends to 1 MHz. Top panel: differential spectrum (inverse grayscale). Middle panel: dynamic (intensity) spectrum. The frequency–time plots from the linear fits to the front trajectories of the associated CMEs and the density model presented in Section 3.2, for the fundamental and harmonic (thick-dotted curves) plasma emission are overlaid on the spectra (see Figure 9 for details on these curves). Bottom panel: the profiles of GOES SXR 1 – 8 Å (solid black line) and 0.5 – 4 Å (thick-dotted magenta line) flux.

X-class flares and 21 with M-class, with only five events related to C-class flares. This represents a significant deviation with respect to the general GOES SXR flare distribution studied by Veronig *et al.* (2002). In general, it is expected that ∼66 % of the SXR flares are of class C, with ∼9.5 % of class M, and just ∼0.7 % of class X. The general case is also consistent with the power-law distribution of the peak SXR flux [I], where the probability density, $p(I) \sim I^{-b}$ with $b \approx 2$ (see Aschwanden and Freeland, 2012).

As regards the CME compact-event association, 32 of these events were trailing CMEs with speeds ∼1400 km s^{-1} on average, with only 11 events having CMEs slower than 1000 km s^{-1} (600 – 900 km s^{-1} range). This deviates significantly from the LASCO CME distribution from 1998 to 2011. The comparison of the distributions is presented in Figure 13. The same CMEs were systematically found in the ∼360° tail of the width distribution (see Figure 14). These fast and wide CMEs are expected to transport the type IV emitting energetic electrons confined within their cavities. Bain *et al.* (2014) calculated that the electrons accelerated during the CME initiation or early propagation phase, trapped in the CME magnetic structure, do not need to be replenished for about four hours. This is consistent with the duration of the compact type IV bursts, which is on average about 106 minutes. Furthermore, 43 compact events were characterized by a CME preceding the associated fast CME by some hours along the same path (similar measured position angle in

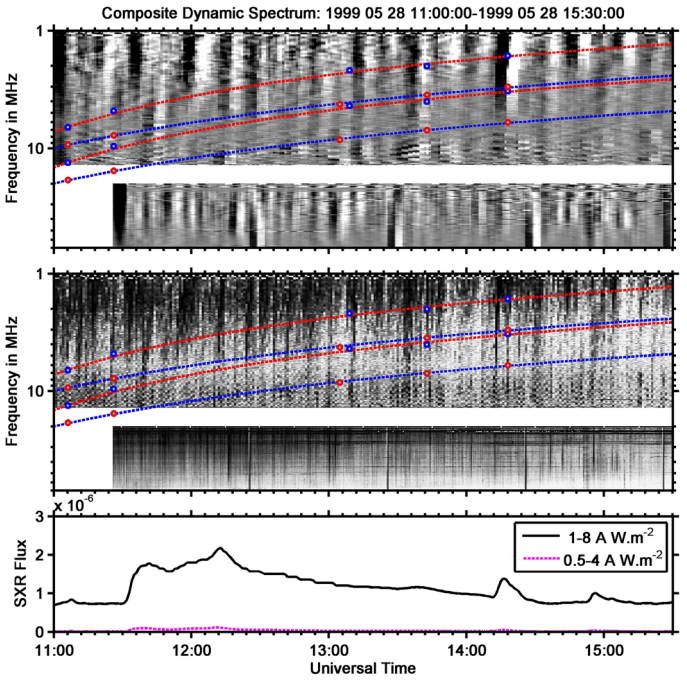

Figure 11 27 – 28 May 1999 event. The panels show the event in the 28 May 11:00 – 15:30 period. The dynamic spectra are combined records from the *Wind*/WAVES and the DAM in the 1 – 70 MHz range. The type IV_{IP} has a coronal extension above 70 MHz; the most prominent part reaches 1 MHz with some parts extending below this frequency. Top panel: differential spectrum (inverse grayscale). Middle panel: dynamic (intensity) spectrum. The frequency–time plots from the linear fits to the trajectories of the associated CMEs and the density model presented in Section 3.2 for the fundamental and harmonic (thick-dotted curves) plasma emission are overlaid on the spectra (see Figure 9 for details on these curves). Bottom panel: the profiles of GOES SXR 1 – 8 Å (solid black line) and 0.5 – 4 Å (thick-dotted magenta line) flux.

the LASCO CME Catalog), which could have reduced the propagation drag on the trailing CME.

During the interval from 28 October 2003 at 11:30 UT to 29 October at 10:17 UT, no CME was reported in the SOHO/LASCO catalog, but two type IV_{IP} bursts, in close succession, were recorded by the *Wind*/WAVES. These correspond to entries 28 and 29 in the attached online table and represent two compact events associated with M-class flares. In the column with remarks of the LASCO CME Catalog, the line corresponding to the 28 October 2003 11:30 halo CME and the associated X17.2 flare reports that "all images after 13:00 UT, particularly C3, are severely degraded due to the ongoing proton storm". The non-detection of CMEs associated with the events on 28 and 29 October might therefore be due to this fact.

4.2. Characteristics of the Three Extended Events

The three extended or long-duration type IV_{IP} events seem to need a resupply of the continuum because they lasted from 960 min to 115 hours (examples in Figures 5 and 9); this requirement holds regardless of the intensity and speed of the first associated flare-CME event. The energetic electron sources in the corona manifest themselves as metric–

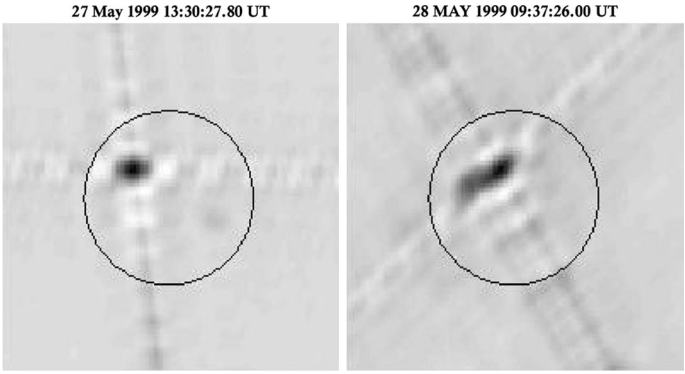

Figure 12 Positions of the coronal type IV bursts in the 27 – 28 May 1999 period, obtained with the *Nançay Radioheliograph* at 164 MHz.

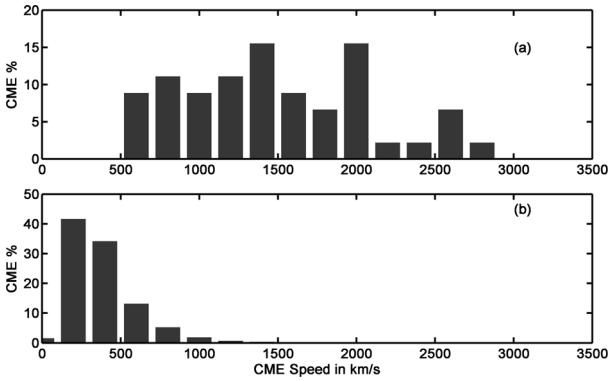

Figure 13 Distribution (%) of CME speeds. (a) LASCO CMEs associated with compact events. (b) All LASCO CMEs in the 1998 – 2012 period for comparison.

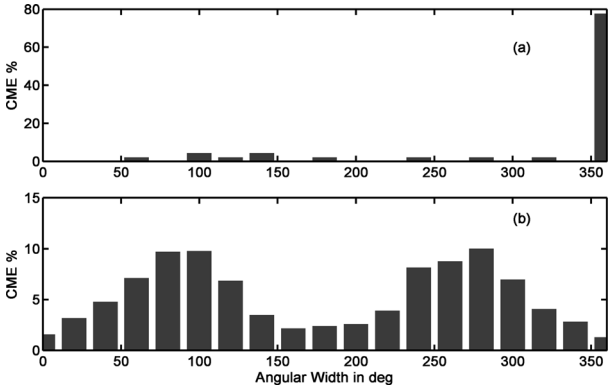

Figure 14 Distribution (%) of CME widths. (a) LASCO CMEs associated with compact events. (b) All LASCO CMEs in the 1998 – 2012 period for comparison.

decametric type III and type IV radio bursts. These electron sources need be associated with the lift-off and propagation of CMEs because they deform the solar magnetic field, providing a propagation path for the energetic electrons, and, at the same time, a moving magnetic trap.

In the examples of extended interplanetary type IV bursts discussed in Sections 3.4, 3.5, and 3.6, we see the replenishment process, mentioned above, at work. In all cases we have, in addition to the dynamic spectra, a partial coverage with NRH images. The energetic electron sources in the corona, manifesting themselves as metric and decametric type IV radio bursts, persist in the same position for the duration of each of the interplanetary type IV bursts.

There are other possible sources of energetic electrons, however. First are the type III bursts. They appear to extend in the dynamic spectra far beyond the low-frequency limits of the type IV_{IP} bursts; therefore, a mechanism of electron deposition into the type IV_{IP} is not easily envisaged. The type III-like activity, however, embedded within the type IV continua as part of the type IV fine structure, is linked to the type IV energetic population and the corresponding acceleration process. Another kind of type III-like activity are the micro-type III bursts, which are parts of the IP storms. As they are significantly weaker than the standard type III (six orders of magnitude, see Morioka *et al.*, 2007), they are difficult to detect, especially in their presence, but they cannot be ruled out.

The second possible source is the type IV_{IP} replenishment from the shock-accelerated electrons. The type II bursts mostly appear piston driven by CMEs and preceding the type IV continuum, interplanetary and coronal, which evolves in their wake, possibly within the CME core. This implies a sort of magnetic isolation from energetic populations in the vicinity of the CME bow shock. We note, however, that the possibility of acceleration in the low corona by shocks distinct from those preceding the type IV burst cannot be precluded; the observational confirmation is difficult, however, as these are often buried in other types of radio activity.

5. Discussion and Conclusions

The present study is based on a multi-frequency and multi-instrument study of a sample of 48 interplanetary type IV (type IV_{IP}) bursts identified from the *Wind*/WAVES on line catalog. The dynamic spectra obtained from the *Wind*/WAVES R1 and R2 receivers in the hectometric frequency range are combined with metric and decametric dynamic spectra and supplemented with GOES SXR light curves and LASCO CME data.

In most cases, 45 out of 48, the extension of a metric–decametric moving type IV burst in the hectometric frequency range is found to be associated with a fast and wide CME (see Section 4.1) capable of driving the embedded type IV source into the high corona. This type of bursts has a duration of about 106 minutes on average; these bursts are dubbed compact type IV_{IP} bursts. The reduced aerodynamic drag in the wake of a previous CME, along the same propagation path, appears to increase the probability of the appearance of a type IV_{IP} burst. This preconditioning of the interplanetary space by a previous CME was first proposed, before the discovery of CMEs, by Caroubalos (1964), who stated that a disturbance following a preceding disturbance encounters much more regular conditions than the first. This result points to the effect of CMEs on the structure of the ambient magnetic field and solar wind flow, which in turn controls the propagation behavior of trailing CMEs, as discussed in a number of publications (Vršnak and Žic, 2007; Gopalswamy, 2008; Baker *et al.*, 2013; Vršnak *et al.*, 2014; Liu *et al.*, 2014; Temmer and Nitta, 2015). The basic argument in all cases is that a CME can be subjected to a minimal slowdown in the wake of a preceding CME, as it encounters a preconditioned region of depleted ambient plasma density and almost radial magnetic field lines; within this region, a reduced aerodynamic drag is expected. The efficiency of this effect increases, possibly, if the main CME is quite dense (as discussed by Temmer and Nitta, 2015, based on detailed modelling of a CME propagation). It is also

expected that a wide preceding CME would result in a greater drop of the aerodynamic drag compared to a narrow CME along the path of the main CME. Further complications may arise when there is more than one CME preceding the main one as regards CME paths and speeds and the ambiguities in CME mass calculations. Despite these, our results provide qualitative support to the reduced aerodynamic drag postulated by the preconditioning hypothesis.

In addition to the preconditioning of space by a preceding CME that we have discussed in the previous paragraph, the characteristics of these events are consistent with the big flare syndrome since they were mostly associated with medium to large flares and fast CMEs (see Section 4.1). As regards the small number (five of 45) of events associated with smaller flares, we find that either the type IV burst was originating at the solar limb (numbers 37 and 44 in the attached table), or (numbers 35, 42, and 43) the origin of the flare was not known; in both cases the flare association was quite uncertain. There were also intense flares within the period of interest, 1998 – 2012, which did not give type IV_{IP} bursts. This may at least in part be explained by the fact that in the *Wind*/WAVES catalog some events are not listed as type IV bursts. On 20 January 2005, for example, the interplanetary radio signature of the X7.1/2B flare accompanied by a fast ($\approx$900 km s^{-1}) halo CME was described as very diffuse. The same holds for the major solar eruption of 7 March 2012 (X5.4 and X1.3 flares associated with two fast ($>$2000 km s^{-1}) CMEs, see Patsourakos *et al.*, 2013, 2016); the radio signature is mentioned as strong intermittent multiple tones.

In the three long-duration or extended type IV_{IP} bursts, the energetic electron population, which is the type IV_{IP} source, seems to be replenished from the lower solar corona. This implies the possibility that the type IV_{IP} enclosing magnetic structure is connected to low coronal electron accelerators or coronal reservoirs. The NRH images, when available, indicate that these might be associated with the high-frequency type IV that persists throughout the duration of the extended type IV_{IP} burst.

A steady coronal reservoir of energetic electrons appears to be the metric type IV continuum because most of the type IIIs tend to overshoot the interplanetary type IV. The micro-type III bursts, on the other hand, may trace the electrons' path from the coronal reservoir to the type IV_{IP}. We state at this point that the term coronal reservoir is used to distinguish this region from the heliospheric reservoirs (see Roelof *et al.*, 1992; Sarris and Malandraki, 2003) beyond 1 AU. The fact that the extended type IV_{IP} bursts appear to cumulatively result from relatively small energetic events suggests the presence of some type of trapping structure for the exciter energetic electrons. The type IV_{IP} heliocentric distances, however, are $\sim$25 – 95 $R_{\odot}$, which are much smaller than the distance of 1 AU and beyond of the heliospheric reservoirs. The question of the confinement of the energetic electrons that produce this type of bursts at heliocentric distances on the order of some tens of solar radii remains open.

Acknowledgements This research has been partly cofinanced by the European Union (European Social Fund, ESF) and Greek national funds through the Operational Program Education and Lifelong Learning of the National Strategic Reference Framework (NSRF) – Research Funding Program: Thales. Investing in society knowledge through the European Social Fund. The LASCO CME Catalog is generated and maintained at the CDAW Data Centre by NASA and The Catholic University of America in cooperation with the Naval Research Laboratory. SOHO is a project of international cooperation between ESA and NASA. The *Nançay Radioheliograph* (NRH) is operated by the Observatoire de Paris and funded by the French research agency CNRS/INSU. *The Radio Solar Telescope Network* (RSTN) is a network of solar observatories maintained and operated by the U.S. Air Force Weather Agency. The authors acknowledge the use of the smoothed differentiation filter software by Jianwen Luo. They also thank the anonymous referee for valuable comments and useful suggestions.

Disclosure of Potential Conflicts of Interest The authors declare that they have no conflicts of interest.

Appendix: Comprehensive Catalog of the Type IV_{IP} Burst Records

In Table 1, which is attached as online supplementary material, we provide a summary of the interplanetary type IV bursts recorded by the *Wind*/WAVES R1 and R2 receivers in the 13.825 MHz – 20 kHz frequency range, with their associated CMEs and SXR flares in the 1998 – 2012 period. The coronal extensions of these bursts by the RSTN, DAM, ARTEMIS-IV, *Culgoora*, *Hiraiso*, and IZMIRAN *Radio Spectrographs* are included for comparison.

The headline to each event includes the event number, date of observation, and characterization of the event as compact or extended following the classification introduced in Section 3. Column 1 lists the type of activity; for SXR flares we list the GOES class. The secondary headline, CME preceding main ejection, stands for CMEs preceding the main CME associated with the event by approximately two days along the same path. The path similarity is determined by the comparison of the position angle (PA) and width of the preceding CME to the main. In the extended events, the secondary headline is sometimes absent as they may originate from a number of energetic events (flares and CMEs) and not from a powerful flare or fast CME with the latter propagating in the wake of preceding ejections (see discussion in Section 5). Columns 2 – 3 list start, peak, and end of each type of activity in day, month, hour, and minute (DD MMM HH:MM) format. D indicates that the event extends in time beyond the observation period. The CME start time, in the second column, is the first C2 appearance, while its extrapolated lift-off time appears in the next row as a remark (see below for the description of the remark lines). In the fourth column, we list the SXR flare 1 – 8 Å integrated flux (F^{tot}_{SXR} in $J\,m^{-2}$), and in the same column, the CME speed (V_{CME}) in $km\,s^{-1}$. The location of the flare on the disk and the measured position angle (MPA) of the CMEs with their angular widths in parenthesis are given in the fifth column. The SXR flare location is determined from the position of the associated Hα flare on the disk or the *Solar X-ray Imager* of GOES report if available. In the fifth column, we also report the position of the coronal radio bursts when NRH records are available. In the sixth column we list the frequency range of the radio bursts in MHz; L indicates that the burst extends to lower frequencies, H stands for a high-frequency extension.

Comments and remarks, when necessary, are in separate lines below the description of the activity line. The comments include the reporting stations from which the data of each observation were obtained, together with the classification of the *Wind*/WAVES, the SOHO/LASCO records, and the NOAA active region number of the event. For the flares, the SXR peak and the Hα category when available are reported, while for the CMEs the extrapolated lift-off time is presented. Finally, in the comment lines data gaps are reported (if any).

The reporting observatory or space experiment abbreviations used in Table 1 are as follows:

ART-4	ARTEMIS-IV, Greece
CUL	Culgoora, Australia
SAG	RSTN, Sagamore Hill, Massachusetts, USA
PAL	RSTN, Palehua, Hawaii
HOL	RSTN, Holloman, New Mexico, USA
LEA	RSTN, Learmonth, Australia
SVI	RSTN, San Vito, Italy
RAM	Ramey AFB, Puerto Rico, USA
IZM	IZMIRAN *Radio Spectrograph*
KANZ	*Kanzelhöhe Solar Observatory*

MIT *National Astronomical Observatory of Japan*, Mitaka
HiRAS *Hiraiso Radio Spectrograph*
DAM *Nançay Decameter Array*
NRH *Nançay Radioheliograph*
XFL SXR flare from the GOES *Solar X-ray Imager* (SXI)
Gxx SXR flare from the GOES (for example G08 stands for GOES 08)

All abbreviations, with the exception of NRH, DAM, and ART-4, are adopted from the Space Weather Prediction Center[11] station list.

References

Alissandrakis, C.E., Nindos, A., Patsourakos, S., Kontogeorgos, A., Tsitsipis, P.: 2015, *Astron. Astrophys.* **582**, A52. DOI.
Aschwanden, M.J., Freeland, S.L.: 2012, *Astrophys. J.* **754**, 112. DOI.
Aurass, H., Vršnak, B., Mann, G.: 2002, *Astron. Astrophys.* **384**, 273. DOI.
Aurass, H., Vourlidas, A., Andrews, M.D., Thompson, B.J., Howard, R.H., Mann, G.: 1999, *Astrophys. J.* **511**, 451. DOI.
Bain, H.M., Krucker, S., Saint-Hilaire, P., Raftery, C.L.: 2014, *Astrophys. J.* **782**, 43. DOI.
Baker, D.N., Li, X., Pulkkinen, A., Ngwira, C.M., Mays, M.L., Galvin, A.B., Simunac, K.D.C.: 2013, *Space Weather* **11**, 585. DOI.
Bastian, T.S., Pick, M., Kerdraon, A., Maia, D., Vourlidas, A.: 2001, *Astrophys. J.* **558**, L65. DOI.
Benz, A.O.: 1980, *Astrophys. J.* **240**, 892. DOI.
Boischot, A.: 1957, *C. R. Math.* **244**, 1326.
Boischot, A., Rosolen, C., Aubier, M.G., Daigne, G., Genova, F., Leblanc, Y., *et al.*: 1980, *Icarus* **43**, 399. DOI.
Bougeret, J.-L., Fainberg, J., Stone, R.G.: 1983, *Science* **222**, 506. DOI.
Bougeret, J.-L., Fainberg, J., Stone, R.G.: 1984a, *Astron. Astrophys.* **136**, 255.
Bougeret, J.-L., Fainberg, J., Stone, R.G.: 1984b, *Astron. Astrophys.* **141**, 17.
Bougeret, J.-L., Kaiser, M.L., Kellogg, P.J., Manning, R., Goetz, K., Monson, S.J., *et al.*: 1995, *Space Sci. Rev.* **71**, 231. DOI.
Cane, H.V., Reames, D.V.: 1988, *Astrophys. J.* **325**, 895. DOI.
Caroubalos, C.: 1964, *Ann. Astrophys.* **27**, 333.
Caroubalos, C., Maroulis, D., Patavalis, N., Bougeret, J.-L., Dumas, G., Perche, C., *et al.*: 2001, *Exp. Astron.* **11**, 23. DOI.
Delaboudinière, J.-P., Artzner, G.E., Brunaud, J., Gabriel, A.H., Hochedez, J.F., Millier, F., *et al.*: 1995, *Solar Phys.* **162**, 291. DOI.
Fainberg, J., Stone, R.G.: 1970a, *Solar Phys.* **15**, 222. DOI.
Fainberg, J., Stone, R.G.: 1970b, *Solar Phys.* **15**, 433. DOI.
Fainberg, J., Stone, R.G.: 1971, *Solar Phys.* **17**, 392. DOI.
Gergely, T.E.: 1986, *Solar Phys.* **104**, 175. DOI.
Gopalswamy, N.: 2004, In: Gary, D.E., Keller, C.U. (eds.) *Solar and Space Weather Radiophysics: Current Status and Future Developments*, Kluwer Academic, Dordrecht, 305. DOI.
Gopalswamy, N.: 2008, *J. Atmos. Solar-Terr. Phys.* **70**, 2078. DOI.
Gopalswamy, N.: 2011 In: *Proc. 7th Int. Workshop on Planetary, Solar and Heliospheric Radio Emissions (PRE VII)*, Austrian Acad. Sciences Press, Graz, 325.
Gopalswamy, N., Yashiro, S., Michalek, G., Stenborg, G., Vourlidas, A., Freeland, S., Howard, R.: 2009, *Earth Moon Planets* **104**, 295. DOI.
Gorgutsa, R.V., Gnezdilov, A.A., Markeev, A.K., Sobolev, D.E.: 2001, *Astron. Astrophys. Trans.* **20**, 547. DOI.
Guidice, D.A., Cliver, E.W., Barron, W.R., Kahler, S.: 1981, *Bull. Am. Astron. Soc.* **13**, 553.
Hillaris, A., Malandraki, O., Klein, K.-L., Preka-Papadema, P., Moussas, X., Bouratzis, C., *et al.*: 2011, *Solar Phys.* **273**, 493. DOI.
Kahler, S.W.: 1982, *J. Geophys. Res.* **87**, 3439. DOI.
Kayser, S.E., Bougeret, J.-L., Fainberg, J., Stone, R.G.: 1987, *Solar Phys.* **109**, 107. DOI.

[11] ftp.swpc.noaa.gov/pub/welcome/stations.

Kerdraon, A., Delouis, J.-M.: 1997, In: Trottet, G. (ed.) *Coronal Physics from Radio and Space Observations*, *Lect. Notes Phys.* **483**, Springer, Berlin, 192. ISBN 978-3-540-68693-4. DOI.
Klein, K., Mouradian, Z.: 2002, *Astron. Astrophys.* **381**, 683. DOI.
Klein, K., Krucker, S., Lointier, G., Kerdraon, A.: 2008, *Astron. Astrophys.* **486**, 589. DOI.
Kondo, T., Isobe, T., Igi, S., Watari, S., Tokimura, M.: 1995, *J. Commun. Res. Lab.* **42**, 111.
Kontogeorgos, A., Tsitsipis, P., Caroubalos, C., Moussas, X., Preka-Papadema, P., Hilaris, A., *et al.*: 2006a, *Exp. Astron.* **21**, 41. DOI.
Kontogeorgos, A., Tsitsipis, P., Moussas, X., Preka-Papadema, G., Hillaris, A., *et al.*: 2006b, *Space Sci. Rev.* **122**, 169. DOI.
Kontogeorgos, A., Tsitsipis, P., Caroubalos, C., Moussas, X., Preka-Papadema, P., Hilaris, A., *et al.*: 2008, *Measurement* **41**, 251. DOI.
Lecacheux, A.: 2000 In: *Radio Astronomy at Long Wavelengths*, *Geophys. Monograph. Ser.* **119**, AGU, Washington, 321.
Liu, Y.D., Luhmann, J.G., Kajdič, P., Kilpua, E.K.J., Lugaz, N., Nitta, N.V., *et al.*: 2014, *Nat. Commun.* **5**, 3481. DOI.
Magdalenić, J., Marqué, C., Zhukov, A.N., Vršnak, B., Žic, T.: 2010, *Astrophys. J.* **718**, 266. DOI.
Magdalenić, J., Marqué, C., Zhukov, A.N., Vršnak, B., Veronig, A.: 2012, *Astrophys. J.* **746**, 152. DOI.
Morioka, A., Miyoshi, Y., Masuda, S., Tsuchiya, F., Misawa, H., Matsumoto, H., Hashimoto, K., Oya, H.: 2007, *Astrophys. J.* **657**, 567. DOI.
Nindos, A., Aurass, H., Klein, K.-L., Trottet, G.: 2008, *Solar Phys.* **253**, 3. DOI.
Nindos, A., Alissandrakis, C.E., Hillaris, A., Preka-Papadema, P.: 2011, *Astron. Astrophys.* **531**, A31. DOI.
Patsourakos, S., Vlahos, L., Georgoulis, M., Tziotziou, K., Nindos, A., Podladchikova, O., *et al.*: 2013, In: *11th Hellenic Astron. Conf.*, 10.
Patsourakos, S., Georgoulis, M.K., Vourlidas, A., Nindos, A., Sarris, T., Anagnostopoulos, G., *et al.*: 2016, *Astrophys. J.* **817**, 14. DOI.
Pick, M., Vilmer, N.: 2008, *Astron. Astrophys. Rev.* **16**, 1. DOI.
Pohjolainen, S., Hori, K., Sakurai, T.: 2008, *Solar Phys.* **253**, 291. DOI.
Pohjolainen, S., Khan, J.I., Vilmer, N.: 1999, In: Wilson, A., *et al.* (eds.) *Magnetic Fields and Solar Processes*, *ESA* **SP-448**, 991.
Pohjolainen, S., Maia, D., Pick, M., Vilmer, N., Khan, J.I., Otruba, W., *et al.*: 2001, *Astrophys. J.* **556**, 421. DOI.
Pohjolainen, S., van Driel-Gesztelyi, L., Culhane, J.L., Manoharan, P.K., Elliott, H.A.: 2007, *Solar Phys.* **244**, 167. DOI.
Prestage, N.P., Luckhurst, R.G., Paterson, B.R., Bevins, C.S., Yuile, C.G.: 1994, *Solar Phys.* **150**, 393. DOI.
Reiner, M.J., Kaiser, M.L., Fainberg, J., Bougeret, J.-L.: 2006, *Solar Phys.* **234**, 301. DOI.
Robinson, R.D.: 1978, *Aust. J. Phys.* **31**, 533. DOI.
Robinson, R.D.: 1985, In: McLean, D.J., Labrum, N.R. (eds.) *Solar Radiophysics: Studies of Emission from the Sun at Metre Wavelengths*, Cambridge University Press, Cambridge 385.
Roelof, E.C., Gold, R.E., Simnett, G.M., Tappin, S.J., Armstrong, T.P., Lanzerotti, L.J.: 1992, *Geophys. Res. Lett.* **19**, 1243. DOI.
Sakurai, K.: 1974, *Indian J. Radio Space Phys.* **3**, 289.
Sarris, E.T., Malandraki, O.E.: 2003, *Geophys. Res. Lett.* **30**, 2079. DOI.
Temmer, M., Nitta, N.V.: 2015, *Solar Phys.* **290**, 919. DOI.
Usui, S., Amidror, I.: 1982, *IEEE Trans. Biomed. Eng.* **29**, 686. DOI.
Veronig, A., Temmer, M., Hanslmeier, A., Otruba, W., Messerotti, M.: 2002, *Astron. Astrophys.* **382**, 1070. DOI.
Vršnak, B., Cliver, E.W.: 2008, *Solar Phys.* **253**, 215. DOI.
Vršnak, B., Magdalenić, J., Zlobec, P.: 2004, *Astron. Astrophys.* **413**, 753. DOI.
Vršnak, B., Žic, T.: 2007, *Astron. Astrophys.* **472**, 937. DOI.
Vršnak, B., Temmer, M., Žic, T., Taktakishvili, A., Dumbović, M., Möstl, C., *et al.*: 2014, *Astrophys. J. Suppl.* **213**, 21. DOI.
White, S.M.: 2007, *Asian J. Phys.* **16**, 189.
Yashiro, S., Gopalswamy, N., Michalek, G., St. Cyr, O.C., Plunkett, S.P., Rich, N.B., Howard, R.A.: 2004, *J. Geophys. Res.* **109**(18), 7105. DOI.
Zharkova, V.V., Kosovichev, A.G.: 1999, In: Vial, J.-C., Kaldeich-Schü, B. (eds.) *8th SOHO Workshop: Plasma Dynamics and Diagnostics in the Solar Transition Region and Corona*, *ESA* **SP-446**, 755.